Light emission from whispering-gallery modes in microscopic spheres

Michael J. Jory

Thin Film Photonics Group, School of Physics, University of Exeter, Stocker Road, Exeter EX4 4QL, UK

Elaine A. Perkins

Detection, Defence Science and Technology Laboratory, Porton Down, Salisbury, Wiltshire SP4 OJQ, UK

J. Roy Sambles

Thin Film Photonics Group, School of Physics, University of Exeter, Stocker Road, Exeter EX4 4QL, UK

Received April 7, 2003; accepted May 5, 2003

The emission of light from whispering-gallery modes excited in microscopic spheres is examined. An evanescent wave is produced by total internal reflection of an optical beam at a planar glass–air interface. This evanescent wave is used to excite whispering-gallery modes in single microscopic spheres placed behind the glass–air interface. The intensity of light emitted into the air half-space from such spheres is measured as a function of scattering angle for both *p*- and *s*-polarized input beams. These data are compared with a simple theory for the emission from a point source above a planar glass substrate. © 2003 Optical Society of America

OCIS codes: 290.5850, 230.5750, 260.6970, 999.9999.

1. INTRODUCTION

The interaction of optical waves with spherical objects has been a subject of interest since the pioneering work by Mie.[1] Subsequently, his theory has been extended to describe the way a plane wave scatters from a wide range of systems. These include the spectral response of metallic suspensions, the study of atmospheric dust, the theory of the rainbow, and the effects of clouds and fog.[2,3] More recently, there has been interest in the scattering of evanescent waves by microscopic spheres.[4–8] This can produce enhanced scattering characteristics in terms of higher intensity and improved contrast that have proved valuable in the fields of microscopy and optical sensing.[9–22] Evanescent coupling also permits whispering-gallery modes (WGMs) to be excited inside the sphere.[23–29]

A WGM consists of an optical beam being confined and circulating in an equatorial path within a sphere by successive total or near-total internal reflections at the sphere–air interface.[26,29] Typically, a microsphere is placed near (i.e., within one optical wavelength of) one face of a high-refractive-index prism.[23–29] Light incident through the prism at an angle greater than the critical angle associated with the glass–air interface leads to the generation of an evanescent wave that decays exponentially into the air.[30] Placing the sphere in this evanescent field allows WGMs to be excited, with resonance occurring when the optical path length of one orbit is equal to an integer number of optical wavelengths.[23] (Alternatively, coupling may be achieved by means of an optical fiber; see, for example, Ref. 27.) The amount of energy coupled into the WGM is normally controlled by adjusting the frequency and power of the input laser beam along with the distance between the sphere and prism surface.[24,31] Resonance is then observed as either a reduction in the intensity of the light reflected at the prism–air interface[24,31] or an increase in the intensity of light emitted from the sphere into the air half-space.[24,31] (When a fiber coupler is used, resonant coupling to the WGM may also be observed as a reduction in the intensity of light transmitted through the fiber.[27]) As a result of the high confinement of these modes, the theoretical Q value reaches 10^5, even for a small sphere of diameter 5 μm at optical frequencies.[29] Consequently, microsphere resonators have been used as WGM lasers[31,32] and as photonic dots,[33,34] with Q values as high as 10^9 being reported for larger spheres.[25,26] However, when the microsphere is strongly coupled to (i.e., in contact with) the planar dielectric substrate, the Q values associated with the WGM resonances are $\sim 5 \times 10^2$, much lower than the theoretical value for an isolated sphere.[29] This situation is similar to most prism-based biosensing systems (see, for example, Ref. 35) in which a particle that has become attached to the prism surface is detected by observing the light scattered from it. Microsphere resonators strongly coupled to a prism have already been studied by Ishikawa *et al.*,[28,29] who characterized the spatial distribution of light emitted into the prism half-space and compared the data acquired with the predictions of theory.

In this work we use a similar prism–sphere system, but study the light emitted into the air half-space. Emitted intensity is recorded as a function of scattering angle for both *p*- and *s*-polarized incident beams. To describe a sphere-behind-an-interface system, Mie theory must be extended to include refraction and reflection of the incident and scattered fields at the interface.[36] Further-

1084-7529/2003/091785-07$15.00

more, for evanescent wave scattering, the incident field is not constant over the entire sphere and this must also be accounted for in the theory. Here, finite-element methods (see, for example, Ref. 37), finite-difference, time-domain analysis,[38,39] or the discrete-sources method (see, for example, Ref. 40) may be used to model the scattered intensity as a function of scattering angle. However, all these techniques are mathematically complex, and in some cases require substantial computing power. In this work, we demonstrate that a very simple point source model can be used to describe part of the emission pattern for WGMs excited in a microscopic sphere.

2. EXPERIMENTAL

By using the method described in Ref. 41, a single microscopic sphere is placed on the surface of a fusion-drawn glass slide[42] [fusion-drawn glass is chosen as it has low surface roughness (~13 nm)]. The reverse surface of the slide is then refractive-index matched to a modified prism assembly.[41] This prism assembly is now positioned so that the sphere-populated surface of the glass slide is at the center of a rotatable table.[41] A 10 mW, polarized beam (of wavelength 632.8 nm) from a helium–neon laser is then directed through the prism assembly onto the outer surface of the glass slide. By rotating the table, an angle of incidence beyond the glass–air critical angle is selected to generate an evanescent wave. The sphere is then positioned in the center of the (~100 μm diameter) laser beam spot (details are provided in Ref. 41). A photomultiplier tube detector is mounted on a second, motorized, rotating table whose rotation axis coincides with that of the first table. Scattered intensity is now recorded while the scattering angle, measured from the normal to the surface of the glass slide, is incremented from $-90°$ to 90°. Data are acquired for both *p*- and *s*-polarized input beams. The scattering response of the bare, planar, glass surface (i.e., when the sphere has been removed from the beam spot[41]) is also recorded for both input polarizations. The above process is carried out on a 5 μm-diameter glass sphere (refractive index 1.52) for internal angles of incidence of 42° (just beyond the glass–air critical angle), 47°, 50°, and 53°.

Similar measurements are also taken for a single latex sphere (refractive index 1.60) of diameter 1.4 μm. Data are acquired for incident angles of 48.5° and 53° (beyond the glass–air critical angle). A full description of the experimental arrangement is given in Ref. 41.

3. RESULTS AND DISCUSSION

Figure 1 shows experimental data for a 5 μm sphere placed centrally in an optical beam incident at an angle of 42° (just beyond the critical angle associated with the glass–air interface). Graphs 1(a), (b) and 1(c), (d) show data acquired using *p*- and *s*-polarized input beams, respectively. In each case, the solid curve indicates the scattering response of the system. As the beam spot is larger than the sphere, the signal measured here is the result of fields scattered by the sphere and those that have scattered merely from the planar glass substrate. The curves with pluses indicate the intensity profile obtained when the sphere is moved out of the laser beam spot.[41] (In this case, the laser beam strikes an area of the fusion-drawn-glass-slide surface that is not occupied by a sphere.) Thus we have a direct comparison between the scattering response of the sphere and the signal obtained as the result of light scattering from the surface roughness associated with the substrate.

Both the intensity profiles associated with the sphere are characterized by a peak at a scattering angle of 27° that has a broad shoulder extending down to $-15°$. For scattering angles beyond $-60°$, a clear mode structure is observed. It should be noted that the fine structure evident in these and all the experimentally obtained curves is not random noise but is, in fact, a highly repeatable characteristic of the scattering system. Further investigation is required to explain this but it may be due to scattering from the surface roughness associated with the glass substrate coupling with the scattering from the sphere or perhaps to scattering from the surface roughness of the sphere itself. (The large peak in intensity in both curves at scattering angles above 55° arises from the edge of the refracted beam.) Intensity profiles with similar characteristics are shown in Fig. 2 for an incident angle of 47°. (The large peaks in intensity that occur for

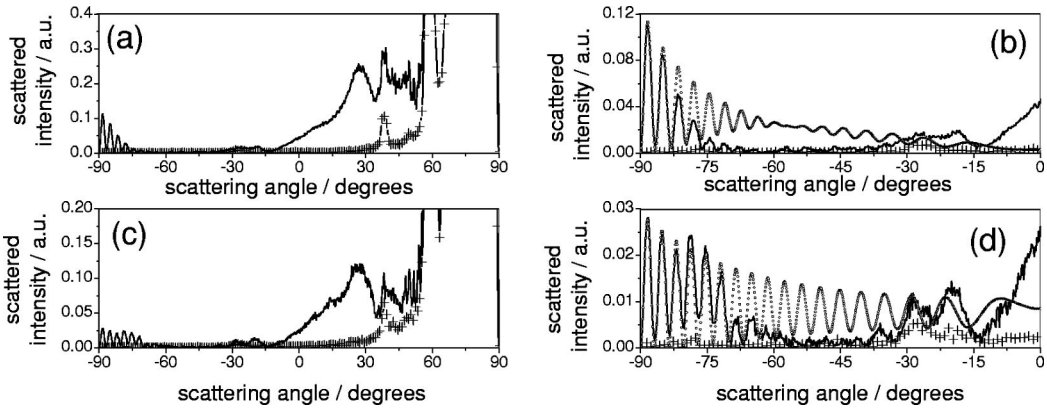

Fig. 1. Scattered intensity versus scattering angle (light-scattering profile) for a 5 μm-diameter glass sphere placed behind a glass–air interface and illuminated with light at an angle of incidence of 42.0° (just beyond the critical angle). Solid and dotted curves are the experimental data and simple model predictions, respectively. The curves with pluses indicate the experimentally measured response of the planar glass surface alone (i.e., with no sphere). (a), (b) *p*-polarized incident beam; (c), (d) *s*-polarized incident beam.

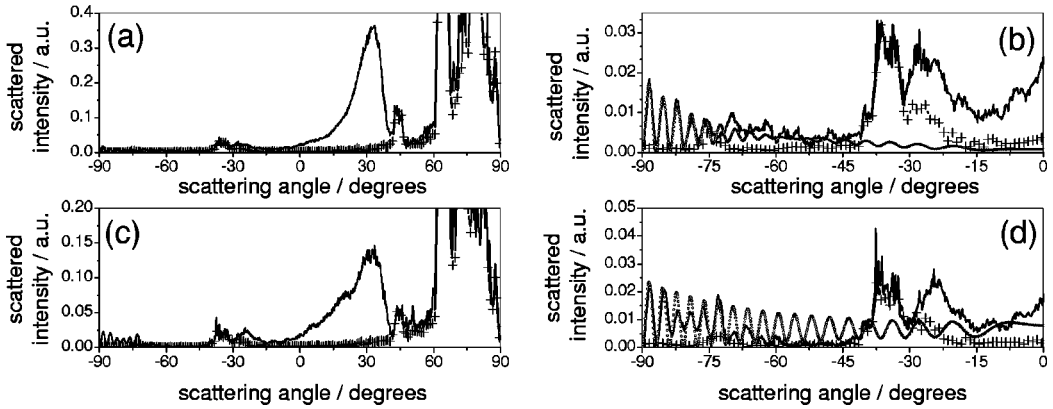

Fig. 2. Light-scattering profile for the same system as in Fig. 1 but illuminated at an angle of incidence of 47.0° (beyond the critical angle). (a), (b) *p*-polarized incident beam; (c), (d) *s*-polarized incident beam.

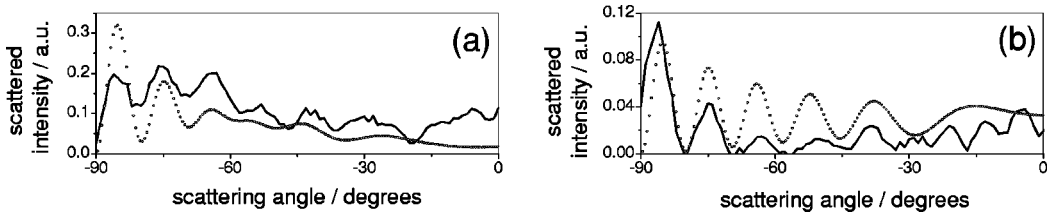

Fig. 3. Light-scattering profile for a 1.4 μm-diameter latex sphere placed behind a glass–air interface and illuminated with light at an angle of incidence of 48.5° (beyond the critical angle). Solid and dotted curves are the experimental data and predicted theory, respectively. (a) *p*-polarized incident beam; (b) *s*-polarized incident beam.

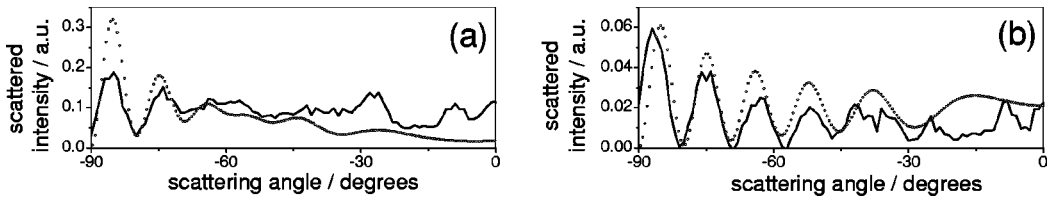

Fig. 4. Light scattering profile for the same system as in Fig. 3 but illuminated at an angle of incidence of 53.0° (beyond the critical angle). (a) *p*-polarized incident beam; (b) *s*-polarized incident beam.

scattering angles above 45° in the data acquired both when the sphere is centered in the laser beam spot and in the background response from the planar glass substrate are due merely to a stray beam that has undergone multiple reflections within the prism.[41]) Similar intensity profiles (not shown) for the same sphere were also obtained for incident angles of 50° and 53°.

Figures 3 and 4 show data acquired (solid curves) for a 1.4 μm-diameter latex bead (refractive index 1.60) placed centrally in an optical beam incident at angles of 48.5° and 53°, respectively (beyond the glass–air critical angle). As there is less scattered intensity from this smaller sphere, the contrast between the sphere and background signals is not as good as for the 5 μm sphere (even after reducing the size of the laser beam spot as described in Ref. 41). The background signal is therefore subtracted from the scattering response acquired for the sphere.[41] Both figures thereby show a clear mode structure that can be associated only with scattering from the sphere.

To understand the electromagnetic response of the samples studied, we have used the High Frequency Structure Simulator computer-modeling software.[37] This software is based on the finite-element method and divides a model of the optical system into a mesh of tens of thousands of tetrahedral volumes, in each element of which the field is represented by a local function. Hence Maxwell's equations are transformed into matrix equations that can be solved with traditional numerical methods. Figure 5 shows a model of a 1.4 μm-diameter sphere of refractive index 1.6 that is surrounded by air. The plane $z = 0$ represents the surface of the glass prism (refractive index 1.52). In the model, *p*-polarized light is injected through the prism from the left at an angle of 45° (beyond the glass–air critical angle). The gray scale represents the magnitude of the electric field evaluated at an instant in time on the plane $y = 0$ (which passes through the center of the sphere). A WGM propagating in a counterclockwise direction is clearly excited around the sphere equator that lies in the $y = 0$ plane (parallel to the plane of incidence). Light emitted from the WGM into the air half-space radiates tangentially to the sphere surface. (Similar results are obtained for an *s*-polarized incident beam.)

Consequently, for scattering angles $0° < \theta < 90°$, it appears that the intensity of light observed in the far field is due only to light emitted directly from the sphere, as indicated by the lack of interference oscillations observed over this angle range (Figs. 1 and 2). However, for scat-

tering angles $-90° < \theta < 0°$, the intensity observed in the far field is the result of the superposition of fields that have been emitted from the sphere at angle θ and those that have radiated at scattering angle $180°-\theta$ and have then been reflected at the air–glass interface. To assess the contribution from each component, the attenuation of the latter upon reflection at the air–glass interface must be accounted for by using the appropriate Fresnel equations.[43] Additionally, the phase difference between the two beams must be calculated.

Figure 6 shows the arrangement of the system for light emitted tangentially to the sphere surface. We now consider a ray emitted directly from the sphere at scattering angle θ (AE in Fig. 6) and a second ray emitted at $180°-\theta$ that is reflected at the air–glass interface (BCD). Now the optical path difference (OPD) can be expressed as

$$\mathrm{OPD} = nAB + BC + CD - AE. \tag{1}$$

Clearly, $AE = FE - FA$ and $CD = GD - GC = FE - GC$

$$\therefore CD - AE = FA - GC, \tag{2}$$

$$nAB = (\pi/2 - \theta)nd, \tag{3}$$

where d and n are the diameter and refractive index of the sphere, respectively. Now,

$$BC = FA = (FC/2) = d(1 + \sin\theta)/2\cos\theta, \tag{4}$$

$$GC = FC\sin\theta = 2BC\sin\theta. \tag{5}$$

From Eq. (1),

$$\mathrm{OPD} = nAB + BC + (CD - AE). \tag{6}$$

Substituting for CD–AE using Eq. (2) yields $\mathrm{OPD} = nAB + BC + FA - GC$, and from Eqs. (3), (4), and (5),

$$\mathrm{OPD} = d[n(\pi/2 - \theta) + \cos\theta]. \tag{7}$$

Figure 7 shows the variation of OPD/d with scattering angle for a glass sphere (solid curve A) and a latex sphere (solid circles, curve B). We now compare these curves with the response for a point-dipole source a distance d above a planar air–glass interface (open circles, curve C). In this case the path difference between the fields directly emitted at angle θ and those that undergo reflection at the planar interface is $2d\cos\theta$ (see, for example, Ref. 2).

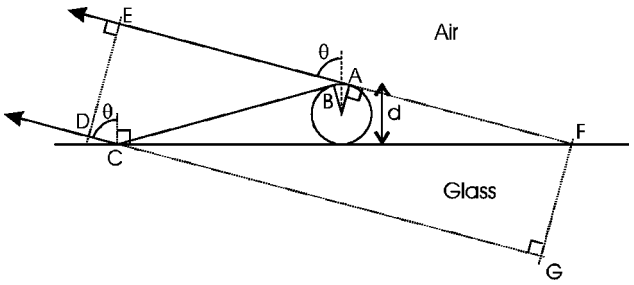

Fig. 6. Ray diagram showing the emission of light from a whispering-gallery mode excited in a sphere of diameter d that is placed behind a glass–air interface. The radiation in the far field is the result of a superposition of fields that are emitted at angle θ (ray AE) and those that are radiated at angle $180°-\theta$ (ray BC) and then reflected at the air–glass interface (ray CD), for scattering angles $-90° < \theta < 0°$.

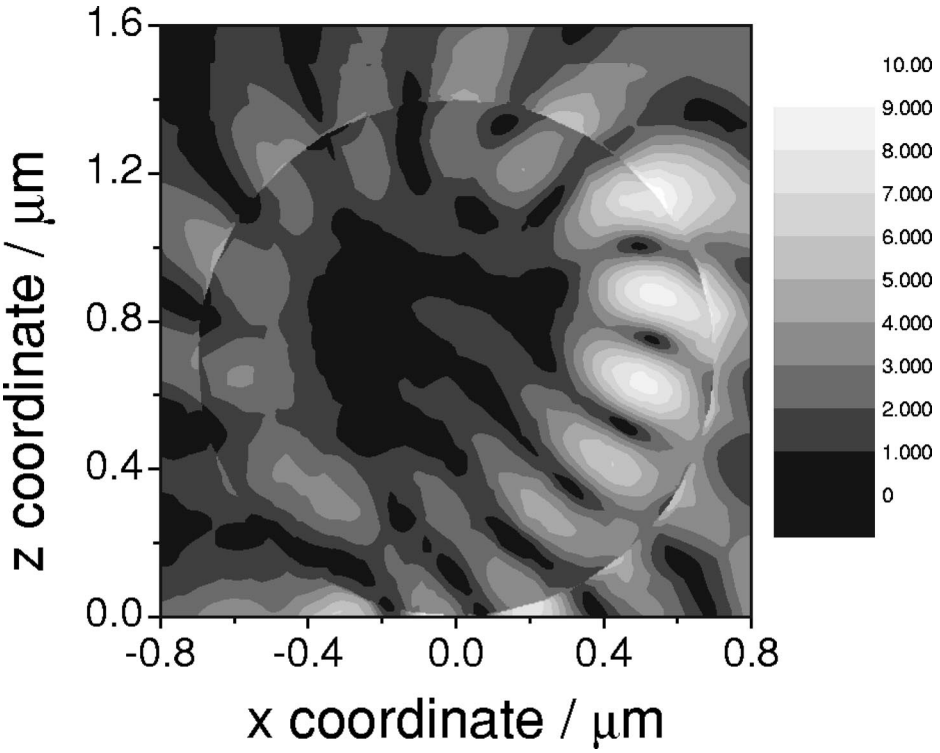

Fig. 5. Model of a 1.4 μm-diameter latex sphere on a planar glass substrate. A p-polarized optical beam strikes the glass–air interface $z = 0$ from the left at an angle of 45° in the glass (beyond the critical angle). The gray scale represents the electric field magnitude (arbitrary units and scale) evaluated at an instant in time on the $y = 0$ plane that passes through the center of the sphere. A whispering-gallery mode propagates in the plane of incidence in a counterclockwise direction around the sphere equator. Light emitted from the whispering-gallery mode radiates largely tangentially to the sphere surface.

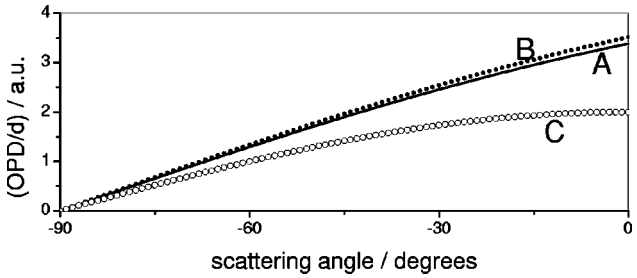

Fig. 7. Optical path difference (OPD) divided by sphere diameter (OPD/d) versus scattering angle for a sphere of refractive index 1.52 (glass) (solid curve A) and refractive index 1.6 (latex) (solid circles curve B). Open circles, curve C, represent the response expected for a point-dipole source surrounded by air and positioned one sphere diameter d above the air–glass interface.

Table 1. Dipole Distances Used in the Simple Modeling to Obtain the Best Fits to Data for the 5 μm-Diameter Glass Sphere

Angle of Incidence (degrees)	Figure	Incident Polarization	Distance of Point Source above Glass Surface (μm $\pm$ 0.01)
42	1(b)	*p*	5.35
42	1(d)	*s*	5.60
47	2(b)	*p*	5.80
47	2(d)	*s*	5.90
50	n/a	*p*	5.50
50	n/a	*s*	5.70
53	n/a	*p*	5.50
53	n/a	*s*	5.70

All three curves show an OPD/d that decreases linearly with scattering angle for angles beyond $-65°$.

We now consider the angle-dependent emission from such a point-dipole source placed above the planar glass surface as predicted by theory. In the model, the dipole is initially oriented so that it is perpendicular to the planar glass surface. The predicted response is then compared with the data acquired with a *p*-polarized beam incident at an angle of 42° [Fig. 1(b)]. To obtain the best fit to the data, the effect of varying the distance of the dipole above the glass surface is investigated. Here, the best agreement is obtained for a distance of 5.35 μm [the dotted curve in Fig. 1(b)]. For scattering angles beyond $-67°$, there is very good agreement between the mode positions and relative peak heights found experimentally and those predicted by this simple model. It should be noted that the scattered intensity predicted by the simple theory is scaled by an arbitrary factor to produce the theory curves shown. As we are comparing only the angular positions and *relative* strengths of the interference oscillations, the absolute strength of the dipole source is not important. The data acquired with an *s*-polarized input beam [Fig. 1(d)] are also compared with the model (dotted curve) with the dipole now perpendicular to the plane of incidence. Here, the dipole is positioned 5.60 μm above the glass surface in the model to obtain the best agreement with experiment. Very good correlation between the angular positions of the modes is observed for scattering angles beyond $-60°$. Both values of dipole position used here are larger than both the given value of sphere diameter (5 μm) and the value measured by experiment in Ref. 41 (5.14 μm). Similar comparisons to theory are shown in Figs. 2(b) and 2(d). (Again, the theory curves are scaled by an arbitrary factor in all cases.) A summary of the values of theoretical dipole position that provide the best fits to data are provided in Table 1. The mean value of dipole position used here, 5.63, is equivalent to $(1.13 \pm 0.01)d$. From Fig. 7, it is clear that the OPD associated with emission from a glass sphere (curve A) is always greater than the OPD associated with the dipole model (using a dipole position of one sphere diameter) (curve C). Therefore, to obtain agreement for $\theta < -65°$ between the two curves, curve C must be scaled by a factor of 1.29. This compares reasonably well with the mean value of dipole position used to fit the experimental data.

We now consider the data acquired for the 1.4 μm-diameter sphere (Figs. 3 and 4). The dotted curves indicate the response predicted by the simple point-dipole model. Again, the distance of the dipole above the planar glass surface is adjusted until the best agreement between data and model is obtained. (For clarity, the model curves are scaled by an arbitrary factor in all cases.) In all cases, the best fits are obtained for a distance of 1.80 μm. This value is larger than both the given value of sphere diameter (1.4 μm) and the value measured by experiment in Ref. 41 (1.5 μm) and is equivalent to $1.29d$. Clearly, the OPD associated with emission from a latex sphere (Fig. 7, curve B) is always greater than the OPD associated with the dipole model (using a dipole position of one sphere diameter) (curve C). In this case, to obtain agreement for $\theta < -65°$ between the two curves, curve C must be scaled by a factor of 1.33. This compares very well with the mean value of dipole position used to fit the experimental data.

4. CONCLUSIONS

In this work, the light emission from whispering-gallery modes excited in single microscopic spheres was studied. Spheres of diameters 5 μm and 1.4 μm (with refractive indices 1.52 and 1.60, respectively) were used, and whispering-gallery modes were excited in each by means of evanescent coupling through a prism. The intensity of light emitted into the air half-space was measured as a function of scattering angle for both *p*- and *s*-polarized input beams. Care was taken to minimize the effects of light scattering from the surface roughness associated with the glass substrate or from surface contaminants as described in Ref. 41. In all cases the scattering response of the sphere was compared to that of the substrate alone.

Modeling the optical response of the system with a finite-element code (High Frequency Structure Simulator[37]) indicates that, as expected, whispering gallery modes are excited around an equator that lies in the plane of incidence. Moreover, light emitted into the air half-space radiates predominantly in a direction tangential to this equator. Consequently, for scattering angles $-90° < \theta < 0°$, the far-field radiation is the result of a superposition of fields emitted directly from the sphere at angle θ and fields emitted at $180° - \theta$ that are then reflected at the planar air–glass interface. The optical

path difference (OPD) between the ray that is directly emitted and the ray that undergoes reflection after emission was then calculated as a function of scattering angle. This was compared to the optical path difference expected for a point source placed one sphere diameter above the air–glass interface. All three curves show that the value OPD/d varies linearly with scattering angle for values of the latter beyond $-60°$.

The scattering angle dependence of the intensity of light emitted from the spheres, as measured by experiment, was then compared to the emission pattern for a point source above a planar air–glass interface, as predicted by a simple model. For high scattering angles, typically beyond $-60°$, very good correlation between the angular position of the intensity peaks was obtained. To obtain the best fits to the data acquired using the glass sphere, the model dipole had to be positioned a mean distance above the air–glass interface of $(1.13 \pm 0.01)d$. This compares reasonably well with the value predicted by a simple optical-path-difference model of $1.29d$. The best fits to the data acquired for a latex sphere were obtained by positioning the dipole $1.29d$ above the substrate, which agrees very well with the value of $1.33d$ predicted by the simple model.

This work has demonstrated that, to first approximation, a simple point-source model may be used to describe the emission patterns (for scattering angles beyond $-65°$) of whispering-gallery modes excited in microscopic spheres. As the spheres used were similar to biological particles in both size and refractive index, this may have important ramifications in the field of optical biosensing.[35]

ACKNOWLEDGMENTS

M. J. Jory gratefully acknowledges funding for a research fellowship under the Joint Grant Scheme from the Defense Science and Technology Laboratory, Porton Down, and the Engineering and Physical Sciences Research Council (UK). The authors also acknowledge the technical help of P. S. Cann.

Corresponding author M. J. Jory may be reached by phone, 1392-264156; fax, 1392-264111; or e-mail, mjjory @exeter.ac.uk.

REFERENCES AND NOTES

1. G. Mie, "Beitrage zur optik truber medien speziell kolloidaler metallosungen," Ann. Phys. (Leipzig) **25**, 377–445 (1908).
2. M. Born and E. Wolf, *Principles of Optics* (Pergamon, New York, 1980).
3. H. C. Van De Hulst, *Light Scattering by Small Particles* (Dover, New York, 1981).
4. C. Liu, T. Weigel, and G. Schweiger, "Structural resonances in a dielectric sphere on a dielectric surface illuminated by an evanescent wave," Opt. Commun. **185**, 249–261 (2000).
5. R. Wannemacher, A. Pack, and M. Quinten, "Resonant absorption and scattering in evanescent fields," Appl. Phys. B **68**, 225–232 (1999).
6. A. V. Zvyagin and K. Goto, "Mie scattering of evanescent waves by a dielectric sphere: comparison of multipole expansion and group-theory methods," J. Opt. Soc. Am. A **15**, 3003–3008 (1998).
7. C. Liu, T. Kaiser, S. Lange, and G. Schweiger, "Structural resonances in a dielectric sphere illuminated by an evanescent wave," Opt. Commun. **117**, 521–531 (1995).
8. D. C. Prieve and J. Y. Walz, "Scattering of an evanescent surface-wave by a microscopic dielectric sphere," Appl. Opt. **32**, 1629–1641 (1993).
9. D. C. Prieve, F. Lanni, and F. Luo, "Brownian-motion of a hydrosol particle in a colloidal force-field," J. Chem. Soc., Faraday Trans. 1 **83**, 297–307 (1987).
10. D. C. Prieve and N. A. Frej, "Total internal-reflection microscopy—a quantitative tool for the measurement of colloidal forces," Langmuir **6**, 396–403 (1990).
11. M. A. Brown, A. L. Smith, and E. J. Staples, "A method using total internal-reflection microscopy and radiation pressure to study weak interaction forces of particles near surfaces," Langmuir **5**, 1319–1324 (1989).
12. I. Braslavsky, R. Amit, B. M. J. Ali, O. Gileadi, A. Oppenheim, and J. Stavans, "Objective-type dark-field illumination for scattering from microbeads," Appl. Opt. **40**, 5650–5657 (2001).
13. G. A. Schumacher and T. G. M. Vandeven, "Evanescent wave scattering studies on latex-glass interactions," Langmuir **7**, 2028–2033 (1991).
14. Z. M. Xia and T. G. M. Vandeven, "Adhesion kinetics of phosphatidylcholine liposomes by evanescent wave light-scattering," Langmuir **8**, 2938–2946 (1992).
15. M. Polverari and T. G. M. Vandeven, "Electrostatic and steric interactions in particle deposition studied by evanescent-wave light-scattering," J. Colloid Interface Sci. **173**, 343–353 (1995).
16. W. J. Albery, G. R. Kneebone, and A. W. Foulds, "Kinetics of colloidal deposition studied by a wall-jet cell," J. Colloid Interface Sci. **108**, 193–198 (1985).
17. W. J. Albery, R. A. Fredlein, G. R. Kneebone, G. J. O'Shea, and A. L. Smith, "The kinetics of colloidal deposition under conditions of controlled potential," Colloids Surf. **44**, 337–356 (1990).
18. B. Mizaikoff, "Mid infra-red evanescent wave sensors—a novel approach for subsea monitoring," Meas. Sci. Technol. **10**, 1185–1194 (1999).
19. C. Malins, M. Landl, P. Simon, and B. D. MacCraith, "Fibre optic ammonia sensing employing novel near infrared dyes," Sens. Actuators B **51**, 359–367 (1998).
20. L. T. Gao, C. J. Seliskar, and L. Milstein, "Spectroscopic sensing with a highly transparent, ion-exchangeable polymer blend," Appl. Spectrosc. **51**, 1745–1752 (1997).
21. G. O'Keeffe, B. D. MacCraith, A. K. McEvoy, C. M. McDonagh, and J. F. McGilp, "Development of a LED-based phase fluorometric oxygen sensor using evanescent-wave excitation of a sol-gel immobilised dye," Sens. Actuators B **29**, 226–230 (1995).
22. S. McCabe and B. D. MacCraith, "Novel mid infra-red LED as a source for optical-fiber gas-sensing," Electron. Lett. **29**, 1719–1721 (1993).
23. R. J. Chang and A. J. Chamillo, *Optical Processes in Microcavities* (World Scientific, Singapore, 1996).
24. S. Schiller and R. L. Byer, "High-resolution spectroscopy of whispering gallery modes in dielectric spheres," Opt. Lett. **16**, 1138–1140 (1991).
25. L. Collot, V. Lefevre-Seguin, M. Brune, J. M. Raimond, and S. Haroche, "Very high-Q whispering-gallery mode resonances observed on fused-silica microspheres," Europhys. Lett. **23**, 327–334 (1993).
26. M. L. Gorodetsky and V. S. Ilchenko, "High-Q optical whispering-gallery microresonantors—precession approach for spherical mode analysis and emission patterns with prism couplers," Opt. Commun. **113**, 133–143 (1994).
27. M. Cai, O. Painter, and K. J. Vahala, "Observation of critical coupling in a fiber taper to a silica-microsphere whispering-gallery mode system," Phys. Rev. Lett. **85**, 74–77 (2000).
28. H. Ishikawa, H. Tamaru, and K. Miyano, "Observation of a modulation effect caused by a microsphere resonator

strongly coupled to a dielectric substrate," Opt. Lett. **24**, 643–645 (1999).
29. H. Ishikawa, H. Tamaru, and K. Miyano, "Microsphere resonators strongly coupled to a plane dielectric substrate: coupling via the optical near field," J. Opt. Soc. Am. A **17**, 802–813 (2000).
30. E. Hecht, *Optics* (Addison-Wesley, London, 1987), p. 107.
31. V. Sandoghdar, F. Treussart, J. Hare, V. Lefevre-Seguin, J. M. Raimond, and S. Haroche, "Very low threshold whispering-gallery-mode microsphere laser," Phys. Rev. A **54**, R1777–R1780 (1996).
32. K. W. An, "Cylindrical and spherical microcavity lasers based on evanescent-wave-coupled gain," J. Chin. Chem. Soc. (Taipei) **48**, 461–468 (2001).
33. M. V. Artemyev and U. Woggon, "Quantum dots in photonic dots," Appl. Phys. Lett. **76**, 1353–1355 (2000).
34. R. Jia, D. S. Jiang, P. H. Tan, and B. Q. Sun, "Quantum dots in glass spherical microcavity," Appl. Phys. Lett. **79**, 153–155 (2001).
35. E. A. Perkins and D. J. Squirrell, "Development of instrumentation to allow the detection of microorganism-susing light scattering in combination with surface plasmon resonance," Biosens. Bioelectron. **14**, 853–859 (2000).
36. G. Videen, "Light-scattering from a sphere behind a surface," J. Opt. Soc. Am. A **10**, 110–117 (1993).
37. High Frequency Structure Simulator computer-modeling software supplied by Ansoft Corporate Headquarters, Four Station Square, Suite 200, Pittsburgh, Pa. 15219-1119.
38. A. Shinya and M. Fukui, "Finite-difference time-domain analysis of the interaction of Gaussian evanescent light with a single dielectric sphere or ordered dielectric spheres," Opt. Rev. **6**, 215–223 (1999).
39. A. Taflove, *Computational Electrodynamics: The Finite-Difference Time-Domain Method* (Artech House, Boston, 1995).
40. Y. Eremin and N. Orlov, "Modeling of light scattering by non-spherical particles based on discrete sources method," J. Quant. Spectrosc. Radiat. Transf. **60**, 451–462 (1998).
41. M. J. Jory, E. A. Perkins, and J. R. Sambles, "Light scattering by microscopic spheres behind a glass–air interface," J. Opt. Soc. Am. A **20**, 1589–1594 (2003).
42. Corning 7509 fusion-drawn glass supplied by Gooch and Housego Ltd., The Old Magistrates Court, Ilminster, Somerset, TA19 OAS, UK. http://www.goochandhousego.com.
43. E. Hecht, *Optics* (Addison-Wesley, London, 1987), p. 94.